The Journal of Experimental Biology 215, 3266-3280

doi:10.1242/jeb.070813

RESEARCH ARTICLE

The active electrosensory range of *Gymnotus omarorum*

Ana Carolina Pereira, Pedro Aguilera and Angel A. Caputi*

Department of Integrative and Computational Neurosciences, Instituto de Investigaciones Biológicas Clemente Estable, Av. Italia 3318, Montevideo, CP 11600, Uruguay

*Author for correspondence (caputiangel@gmail.com)

SUMMARY

This article reports a biophysical and behavioral assessment of the active electrolocation range of *Gymnotus omarorum*. Physical measurements show that the stimulus field of a point on the sensory mosaic (i.e. the potential positions in which an object may cause a significant departure of the transcutaneous field from basal in the absence of an object) consists of relatively extended volumes surrounding this point. The shape of this stimulus field is dependent on the position of the point on the receptive mosaic and the size of the object. Although the limit of stimulus fields is difficult to assess (it depends on receptor threshold), departure from the basal field decays rapidly, vanishing at about 1.5 diameters for conductive spheres. This short range was predictable from earlier theoretical constructs and experimental data. Here, we addressed the contribution of three different but synergetic mechanisms by which electrosensory signals attenuate with object distance. Using novelty responses as an indicator of object detection we confirmed that the active electrosensory detection range is very short. Behavioral data also indicate that the ability to precisely locate a small object of edible size decays even more rapidly than the ability to detect it. The role of active electroreception is discussed in the context of the fish's habitat.

Key words: active senses, reafference, detection, ROC curve, sensory scene, electric image.

Received 30 January 2012; Accepted 30 May 2012

INTRODUCTION

Electroreception is a sensory modality widely distributed in aquatic animals. Many fish species evolved electroreceptors distributed on their skins that sense the transcutaneous patterns of electric current [the so-called 'electric image' (Bastian, 1986)], informing the animal about the nearby environment (Bullock et al., 1961; Bullock and Heiligenberg, 1986; von der Emde and Engelmann, 2011).

Fish electroreception has two modes: passive and active. In passive electroreception, the currents exciting the electroreceptors are generated by other living animals or plants (Kalmijn, 1974). In active electroreception, the discharge of the fish's electric organ (EOD) generates an electric field to 'illuminate' the nearby environment (Bennett, 1971). Non-electrogenic objects differing in impedance from the surrounding water become polarized, imprinting a change on the electric field. The object's effect on the basal electric field can be considered as a signal emitted by the object and received at the skin of the fish (Lissmann and Machin, 1958). Under this view, it is implicit that there is a double effect of distance in active electroreception. According to these authors, 'In the absence of a suitable word to describe quantitatively the effect of an object on an electric field, the word "imprimence" has been coined. It is derived from "impriment" ("something that impresses or imprints") with an ending denoting quantitative measure (cf. "capacitance")'. They also referred to the object-perturbing field as the effect of the 'imprimence' on the electric field (Lissmann and Machin, 1958).

This theory, implicit from the beginning, has persisted over the years and has been reviewed in a seminal paper that compares the characteristic features of electroreception with other sensory modalities (Nelson and MacIver, 2006). In this review the authors state that, 'In teleceptive active sensing of small targets, geometric spreading costs are paid twice, once as energy is propagated from the emitter to the target and again as energy is returned from the target to the receiver' (Nelson and MacIver, 2006). In specific reference to electrolocation they remark that, 'geometric spreading can be modeled using the electrostatic fields of two dipole sources.… Given that spreading costs must be paid twice, the signal intensity that is returned to the receiver would be expected to fall as the sixth power of distance' (Nelson and MacIver, 2006). They further explain why the intensity of the electric image of an object 'electrically illuminated' by a real fish in an aquarium does not decay with the sixth power of the distance. The presence of aquarium borders and the distributed nature of the electric organs cause a reduction of the exponent of the power function from –6 to –1 close to the fish body and to –4 at the far field (Knudsen, 1975; Bastian, 1981a; Bastian, 1981b; Chen et al., 2005; Nelson and MacIver, 2006).

An important contribution to the reduction of the exponent in the juxta-cutaneous space is the inextricable presence of the fish's body (Migliaro et al., 2005; Pereira and Caputi, 2010). As any high conductive elongated object, the fish's body funnels the field along its main axis, concentrating the 'illuminating field' in the neighborhood of the rostral pole where an electrosensory fovea has been described (Caputi and Budelli, 1995; Caputi and Budelli, 2006; Castelló et al., 2000; Aguilera et al., 2001; Migliaro et al., 2005).

This double-distance theory was previously stated in an explicit way in the finite element models of active electrolocation of *Gnathonemus petersii* (Caputi et al., 1998; Budelli and Caputi, 2000) and in theoretical articles on active electroreception (Caputi, 2004; Caputi and Budelli, 2006). Finite element models calculated the electric images and the electric field generated by a fish taking a direct approach from the measured electric source characteristic

curve, the resistivity of the passive tissues and the geometry of the body. In these models the object was represented by its equivalent electric source [see the appendix in Budelli and Caputi (Budelli and Caputi, 2000)]. Thus, this double-distance theory led to a new operative concept for analyzing image formation: the 'electric stamp' of the object. The electric stamp of an object corresponds to the set of electric sources that, if placed instead of the object, yields the same image (Caputi et al., 2008; Pereira and Caputi, 2010). Interestingly, theoretical results suggest that the stamp of an object and the object-perturbing field are dependent on different factors and thus they decay with distance at a different rate (Pereira, 2009; Pereira and Caputi, 2010). While aquarium borders and the fish's body conductivity and shape affect both the stamp and the object-perturbing field, the distributed nature of the electric organ mainly affects the stamp (Pereira, 2009; Pereira and Caputi, 2010).

The double-distance theory raises several interesting corollaries related to the problem of active electroreception range. First, the magnitude of the actively generated electric images decays a great deal with distance, predicting a short detection range (Rasnow, 1996; Caputi et al., 1998). This agrees with physiological measurements of the modulation of electroreceptor firing (Bastian, 1981a; Bastian, 1981b; Gómez et al., 2004) and behavioral estimations of active electroreception range in wave gymnotids and pulse mormyrids (Push and Moller, 1979; Nelson and MacIver, 1999; von der Emde, 1999). Perhaps the most elegant analysis of prey detection was made by combining modeling and video recordings in *Apteronotus* (MacIver, 2001). The application of this technique suggests that these fish electrolocate *Daphnia* individuals between 10 and 28 mm from their dorsal aspect (Nelson and MacIver, 1999; MacIver et al., 2001). However, *Daphnia* also emit electric fields, raising the possibility that both active and passive electrolocation systems may be involved in determining the distance threshold (Nelson and MacIver 1999; MacIver et al., 2001). In fact, although the active electrolocation component appeared clear when the water had a different conductivity from the *Daphnia*, the prey was still detected when the water had the same conductivity ($300\,\mu S\,cm^{-1}$) (MacIver et al., 2001).

Second, the attenuation of the perturbing field with distance means that the electric image is blurred as the distance from the object to the fish increases (Bastian, 1986; Rasnow and Bower, 1996; Rasnow, 1996; Caputi et al., 1998; Budelli and Caputi, 2000; Sicardi et al., 2000; Chen et al., 2005; Gómez et al., 2004; Snyder et al., 2007; Babineau et al., 2006; Pereira and Caputi, 2010). This predicts a reduction of the spatial resolution. In the human eye, the section of every photoreceptor and the optic center of the dioptric apparatus of the eye determine the region of space in which a stimulus may stimulate the photoreceptor. This is roughly a cone with a vertex at the optic center and an angle defined by the diameter of the photoreceptor and the distance to the optic center. As in vision, pre-receptor mechanisms of electrolocation consist of the shape and conductance of the tissues that may guide the energy field to the receptors. However, differently from the eye, the geometry of the elongated fish's body is funneling, from caudal to rostral regions, the self-generated and object-perturbing electric fields (Castelló et al., 2000; Aguilera et al., 2001). This determines that the stimulus fields are very different in shape depending on the position of the object relative to the fish.

Third, because of the spreading of the object-perturbing field, the image of even a small object expands with distance (Caputi and Budelli, 1993; Rasnow, 1996; Caputi et al., 1998; Assad et al., 1999; Nelson and MacIver, 1999; Budelli and Caputi, 2000). This may result in an impairment of object shape discrimination during electrolocation. Theoretical constructs indicate that beyond some critical distance, object images are similar to the image of a sphere (Sicardi et al., 2000). These predictions agree with the experimental data (Rasnow, 1996; Stoddard et al., 1999; Assad et al., 1999; Caputi et al., 2011) and led to an interesting series of behavioral experiments showing that a cube might be confused with a more closely placed sphere (von der Emde et al., 1998). The same reasoning allows one to predict that beyond some distance two objects should not be distinguished from a larger one and that location precision should decay with distance (Pereira and Caputi, 2010).

Although active electroreception is sometimes described as a teleceptive sense, previous analysis of the literature indicates that the detection range using active electrolocation for edible prey appears to be very short. Moreover, theoretical predictions suggest that the range for prey location is even shorter.

The aim of the present article is to provide experimental evidence for the evaluation of the active electroreception range. We focused on the following aspects: (a) are stimulus fields similar in shape at different sites of the receptor mosaic; (b) how far does an electric fish detect the presence of an object using active electrolocation; (c) does detection distance depend on object size; and (d) does active electrolocation precision vanish at short distances?

Our study deals with *Gymnotus omarorum* (Richer de Forges et al., 2009), a species in which electrogeneration mechanisms (Macadar, 1993; Caputi, 1999; Caputi et al., 2005), pre-receptor funneling (Caputi and Budelli, 1995; Aguilera et al., 2001), electroreceptor distribution (Castelló et al., 2000; Caputi et al., 2002) and coding (Cilleruelo and Caputi, 2012) are well known.

We explored these aspects with two experimental techniques: (a) by determining the physical stimulus fields of different points on the fish's skin using direct measurements; and (b) by determining the range of active electrosensory detection and spatial discrimination using novelty responses as a sign of a change in the electrosensory environment. We found that stimulus field rapidly attenuated with distance and that the shape of this field differed depending on the position of the receptor at the sensory mosaic and the object size. Consistent with physical studies, behavioral tests showed that detection occurs within a very short range. Discrimination between two objects 10 mm apart vanished beyond 10 mm distance. As theoretically predicted, all these figures are dependent on object characteristics. Stamp increases with object length along the field lines; consequently detection range increases with object size.

MATERIALS AND METHODS

Animals

Experiments were performed on 20 fish (15–30 cm total length) following the guidelines of the CHEA (Comisión Honoraria de Experimentación Animal, ordinance 4332-99, Universidad de la República Oriental del Uruguay). Experiments were approved by the Animal Ethics Committee of the Instituto de Investigaciones Biológicas 'Clemente Estable' (protocol number 001/03/2011). Fish were gathered at Laguna del Cisne (Maldonado, Uruguay), 1–4 months before the experiment, kept in individual aquaria under a natural light cycle and fed with insect larvae. All traumatic or painful procedures were conducted when the fish reached a deep anesthetic plane where the EOD rate was unresponsive to visual, vibratory, electric or nociceptive stimuli. In those experiments in which the fish may experience pain or discomfort, animals were anesthetized with pentobarbital (0.5–1 mg, i.m.), repeated on demand until they reached and maintained an EOD rate below 10 Hz at 20°C and a slow but stable respiration. At the end of

these experiments, animals were killed by an overdose of pentobarbital (10 mg, i.m.).

Stimulus field measurements

The stimulus field of a receptor is the set of potential positions in which an object may stimulate the receptor. Our experimental strategy was to measure the field adjacent to a given point on the skin (local EOD, LEOD) while a sphere was sequentially placed on a given point of a lattice grid (distance between parallel lines, 2 mm; see Fig. 1). Several points on the skin were explored with spheres of different diameter and conductivity (steel or glass, diameters from 8 to 24 mm). The center of the exploring sphere was placed on the intersection points of the reference lattice. The sphere was moved step by step with a resolution below 200 µm using a computer-controlled *x*–*y* plotter (Hewlett-Packard, HP 7015A). We chose spheres because they are center-symmetrical objects and therefore their effect as stimulus objects is not dependent on their orientation along the field lines.

Measurements were always performed with the fish's body straight, halfway between the bottom and the water surface in a 33×48 cm tank filled with 100±10 µS cm^{-1} water to a depth of 10 cm. In order to keep the fish's body straight, we implanted a fine cotton thread along the midline. The thread came out of the body just behind the occiput and at the limit between the caudal and the center-caudal quarters of the fish body. The ends of the thread were firmly attached to two vertical wooden poles held by an iron framework.

Stimulus fields were systematically studied at four points on the skin in three fish (see Figs 1, 3). We used a recording probe consisting of four (50 µm diameter) tungsten enamel-coated electrodes with their blunt tips assembled at non-coplanar points defining orthogonal lines (2 mm apart). We measured the drop of voltage between a reference electrode placed adjacent to the skin and each of three other electrode tips placed along orthogonal directions (longitudinal, transversal and vertical).

Signals were amplified to give at least 12 bit resolution (10–10,000 Hz band pass, A-M systems-1800, Sequim, WA, USA) and digitized at at least 20 kHz per channel. Data acquisition was made in epochs of 500–700 ms, starting 100 ms after the electrode movement ceased. Seven channels were recorded in each experiment: (a) the head-to-tail EOD, recorded between two electrodes placed on the main axis of the fish at opposite ends of the tank; (b) three for the LEOD (longitudinal, transversal and vertical); and (c) the *x*- and *y*-positions of the sphere on the horizontal plane. We performed 3–5 runs of the sphere along the same trajectory. From each position, we selected at least 10 head-to-tail EOD-centered epochs (duration 10 ms) per recording position and peri-EOD averaged them. The LEOD was calculated by dividing the averaged drops in voltage by the inter-electrode distance and grouping the three measurements as a single vector.

For a given receptor point, the stimulus field intensity for each position of the object (x, y) was defined as the square root of the mean squared value of the LEOD vector modulus (r.m.s.LEOD$_o$). Finally, the stimulus field was defined by subtracting the r.m.s.LEOD in the absence of the object (r.m.s.LEOD$_{wo}$) and normalizing by the standard deviation of the r.m.s.LEOD in the absence of the object [s.d.(r.m.s.LEOD$_{wo}$)]:

$$\text{Stimulus field}(x,y) = \frac{\text{r.m.s.LEOD}_o(x,y) - \text{r.m.s.LEOD}_{wo}(x,y)}{\text{s.d.}(\text{r.m.s.LEOD}_{wo}(x,y))} . \quad (1)$$

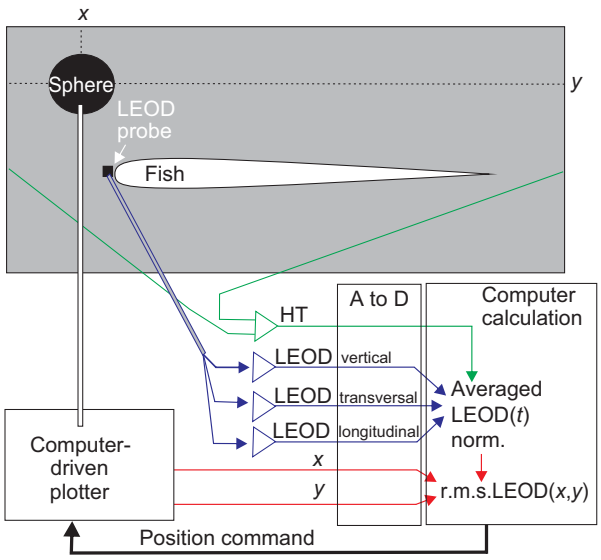

Fig. 1. Experimental setup for recording electric fields. Stimulus field was defined as the departure from the basal electric field at a given point on the skin caused by the presence of an object in any position of space. We restrict this analysis to a horizontal plane passing through the fish at the fovea. We used a 2×2 mm reference lattice for discrete measurements of the stimulus field. At each explored point, we measured the drop of voltage between a reference electrode placed adjacent to the skin and three other electrodes whose tips were placed along orthogonal directions (longitudinal, transversal and vertical, blue channels). A reference head-to-tail (HT) EOD was recorded (green channel). For four local electric organ discharge (LEOD) recording positions on the skin, exploring spheres (black circle) were placed at the intersection points of a Cartesian lattice using a computer-driven plotter. Object coordinates (x, y; red channels) were recorded simultaneously. At each position of the object, an epoch of 500–700 ms including 4–8 EODs was recorded. Waveforms recorded at each channel were peri-event averaged taking as a reference the head-to-tail EOD and the field modulus of this average was calculated [LEOD(t)]. The energy of the signal within a window of 10 ms was estimated as the root mean square (r.m.s.) value of this modulus [r.m.s.LEOD(x,y)]. The stimulus field was defined as the difference between the r.m.s.LEOD(x,y) for each object position and the mean r.m.s.LEOD(x,y) obtained in the absence of the object over the standard deviation of this last value. The fish's body was maintained straight during the whole experiment. A to D, analog to digital.

Measurements of physical parameters involved in image attenuation with distance

The aim of this section of the study was to analyze how object polarization and electric field decay determine the reduction in the amplitude of the electric image with distance.

Object polarization modifies the field generated by the EOD as though a new source were placed on the site of the object. This source is called the 'object's stamp in a given scene' (Caputi et al., 2008; Pereira and Caputi, 2010). In the case of a longitudinal probe, such as the one used in this study, the strength of this source (S) can also be considered proportional to the difference between the object's longitudinal resistance (R_o) and the resistance of an equivalent cylinder of water (R_w):

$$S = I_o(R_o - R_w) . \quad (2)$$

The proportionality constant (I_o) corresponds to the current flowing through the object and can be estimated experimentally by calculating the characteristic curve of the scene 'seen' from the point of view of the object (i.e. Thevenin equivalent characterized by an

electromotive force E_s and a series resistance R_s) (Pereira et al., 2005; Pereira and Caputi, 2010). We experimentally estimated E_s, R_s and S as a function of R_o, R_w and distance (Pereira and Caputi, 2010). To estimate E_s and R_s, we measured the drop of voltage generated by the positive peak of the EOD between the carbon bases of an object probe at different distances from the fish's body. This peak is representative and equivalent to the r.m.s. value as under our recording conditions there is not a significant change in EOD waveform. As voltage (V_o) is an hyperbolic function of object load (R_o), V_o has an asymptotic value equal to E_s when R_o tends to infinity and it is equal to one-half of E_s when R_o=R_s [see appendix in Aguilera et al. (Aguilera et al., 2012)]. Using the following linearization (I_o=V_o/R_o) we were able to easily determine E_s and R_s for each distance from the fish to the probe:

$$V_o = E_s - R_s I_o \,. \quad (3)$$

Then S was estimated as a function of R_o (see Caputi et al., 2008):

$$S = E_s \left[\frac{R_o - R_w}{R_o + R_s} \right] . \quad (4)$$

The attenuation of the object-perturbing field is the same as the attenuation of the field generated by a source placed instead of the object. Thus, it was estimated by measuring the local field on the skin of a fish's cadaver when a sine wave (400 mV peak to peak) was applied between the conductive bases of the probe. We calculated the stamp of the stimulus source (S_e) using the following expression (R_o=0 for a voltage source):

$$S_e = 400 \frac{R_w}{R_s} \,. \quad (5)$$

We measured the peak-to-peak juxta-cutaneous field generated by this sine wave at each distance [JCF(d)] and the attenuation factor as a function of distance [A(d)] as the quotient:

$$A(d) = \frac{\mathrm{JCF}(d)}{S_e} \,. \quad (6)$$

Behavioral experiments

Novelty responses – characterized as a transient acceleration just after a change in the object impedance – proved to be a good index of electrolocation (Caputi et al., 2003; Aguilera et al., 2012). In addition, we have shown that the maximum reduction in the EOD interval (i.e. the amplitude of the novelty response) and the probability of occurrence are good indicators of changes in either the amplitude or the waveform of the local stimuli (Aguilera and Caputi, 2003; Caputi et al., 2003; Pereira et al., 2005). Receiver operating curves (ROC) analysis shows that the probability of occurrence is a good indicator of object detection (see Appendix).

We used novelty responses in two ways. To find the critical distance for object detection we searched for the distance where the probability of evoking a novelty response by maximum changes in object impedance falls below a critical value. To explore the range of location we searched for the distance where the probability of evoking a novelty response by a change in position of a given stamp of the object (mimicking a sudden movement) falls below a critical value.

In both types of experiment we used the same experimental setup [similar to that used previously (Aguilera et al., 2012)]. Fish were kept in a tank containing water at 100±10 μS cm^{-1} (33×48 cm tank filled to a depth of 10 cm), restrained inside a nylon mesh, tightly attached to wooden poles fixed to opposite walls of the tank. The distance between the mesh and the fish was about 1–2 mm. The rostro-caudal movements of the fish were impeded by a piece of cotton on the tail and a piece of the same mesh in front of the jaw. Two electrodes, placed near the wooden supporting poles and connected to a differential amplifier (high input impedance, ×100, 10–10,000 Hz band pass range), were used to record the head-to-tail field generated by the EOD.

Novelty responses were evoked by maximum changes in the object's resistance (2.5 MΩ to 1 kΩ). We used cylindrical probes consisting of a plastic cylinder with carbon bases (von der Emde, 1990; Aguilera and Caputi, 2003). These bases were connected by a resistor of 2.5 MΩ. This resistor was bypassed by another resistor of 1 kΩ, transiently connected at will using a computer-controlled switch (Fig. 2, scheme). Activation of this switch provoked a step reduction of the cylinder longitudinal resistance lasting 2 s. This stimulus was repeated every 30 s (a run) at least 20 times at each position of the object (a trial). Each run started 50 EODs before each resistance step and ended 50 EODs before the next resistance step.

The 30 s interval between changes in object impedance was long enough for to avoid habituation (Aguilera and Caputi, 2003; Caputi et al., 2003; Pereira et al., 2005). We tested the lack of difference of the responses between the first and last run of each trial (difference between medians different from zero, sign test, P<0.01, N=10). Close to the fish, where the probability of novelty responses was 1, we made one or two trials of 20 runs each. As we moved the object away we increased the number of trials in order to better estimate the percentage of evoked novelty responses.

We plotted the rasters of the inter-EOD intervals of first and second order (Fig. 2A, top trace). The first problem that we faced was to define what characteristics of the interval shortening are significant for indicating detection of a local stimulus change. Novelty response implies a sudden acceleration involving in general two or three consecutive reductions of the first-order interval (Fig. 2A, top, black trace) although with exceptionally small (Fig. 2A, top, red trace) or large stimuli (Fig. 2A, top, blue trace), it can range from 1 to 5 intervals. In consequence, the maximal reduction of the second-order interval within a 5 intervals-after-the-step window is the most sensitive parameter for detecting the occurrence of novelty responses. To pinpoint the occurrence of the novelty response, we plotted the rasters of the increment of the second-order interval (Fig. 2A, bottom trace). We calculated the mean and standard deviation of the increment of the second interval and set an arbitrary threshold for defining a novelty response as 2 s.d. below the mean value. Using this criterion we estimated the probability of a novelty response for each distance as the relative frequency (as an estimator of probability) of occurrence at each object position. In order to define a probability level at which there is no detection, we performed a ROC analysis (see Appendix). This analysis indicated that a good criterion was to find the distance where the relative frequency of the novelty response was under 10%.

Experiments for determining the object detection range

We probed the limit of detection along five lines perpendicular to the body (one along the longitudinal axis, two horizontal and two vertical transversal lines perpendicular to the main body axis and at a distance of 15 and 50% of the total length from the snout, Fig. 2B). The axis of the probe was perpendicular to the fish's skin. We explored the responses at different distances from the skin.

To explore the role of object length, we repeated these experiments using two cylinders, a small one of 6 mm diameter and 12 mm length and a large one of 8 and 20 mm, respectively. We

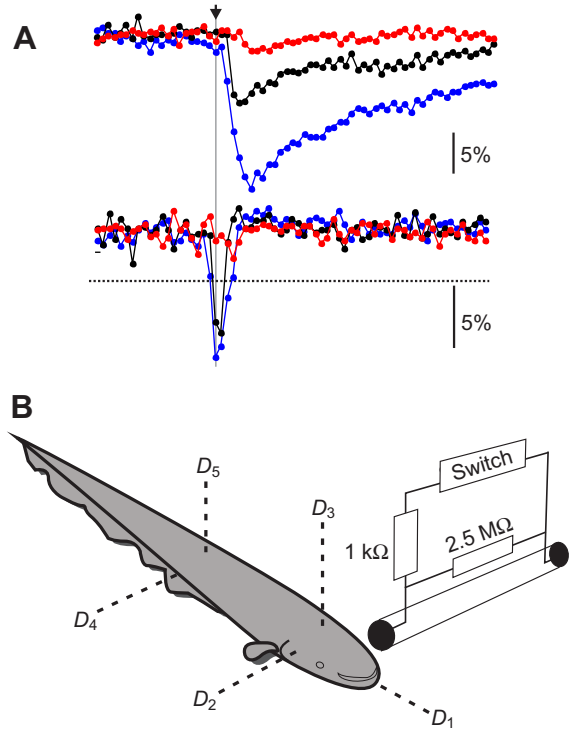

Fig. 2. Experimental setup for behavioral experiments. (A) Fish responded with a step-like reduction in the next two or three inter-EOD intervals to a sudden change in the impedance of the environment (novelty response). We plotted the inter-EOD first interval (top traces) and the increment of the second-order interval (bottom traces) as a function of its starting time. This last raster was the most appropriate to identify the response. The black horizontal dotted line corresponds to one of the sets of arbitrary thresholds used for the receiver operating curves (ROC) analysis. For this particular threshold, the black and blue traces were considered as positive responses, and the red trace as a negative response. Arrow and grey vertical line indicate the switching time of the object resistance. (B) To evoke the novelty responses we used a cylindrical probe consisting of a plastic tube with carbon conductive plugs in both openings. We changed object longitudinal resistance in a step-like manner from 2.5 MΩ to 1 kΩ using a computer-controlled switch. At each position, a series of stimuli each consisting of an object resistance step were performed every 30 s. Five different directions were explored. The probe was placed at different points along lines D_1 to D_5.

increased object diameter as well as length in order to obtain a geometrically equal water cylinder with similar longitudinal resistance (small cylinder 4.2 kΩ, large cylinder 4 kΩ).

Experiments comparing the range of location with the range of detection

We probed the acuity of the system in front of the foveal region in six fish. We used a four-electrode probe with its tips symmetrically located at 5 mm on each side of the midline in the horizontal plane (as if they were pointing to the corners of a 10×20 mm rectangle). Each electrode consisted of a pencil lead (300 µm, graphite) insulated except at 1 mm from the tip. Shunting a longitudinal pair of electrodes with a 1 kΩ resistor causes the emergence of a stamp mimicking the appearance of an object. Simultaneous disconnection of the right electrode pair and shunting of the left electrode pair causes a change in the position of the stamp, mimicking the movement of an object from right to left. In two fish, we searched for the distance where this movement mimicking maneuver evoked novelty responses in less than 10% of the runs and compared this distance with the detection distance obtained by evoking the novelty response by transiently shunting only the right pair of electrodes.

RESULTS

Stimulus fields of different skin locations explored with spheres of different volumes

The stimulus field of a given point on the skin is the region of space where an object causes a LEOD significantly different from the LEOD obtained in its absence. Stimulus fields of selected points of the skin were explored by measuring the LEOD while a sphere was moved step by step in the horizontal plane containing the main axis of the fish. Spheres of different conductivity (steel and glass) and diameter (8–25 mm) were placed step by step at equally spaced points (2 mm) along equally spaced lines (2 mm) parallel to the fish's longitudinal axis. Even if the absolute limit of a stimulus field is arbitrary in the absence of a behavioral correlate, this procedure allowed us to define the regions of the nearby space in which an object caused a similar local stimulus departure from the basal field.

Stimulus fields for a sphere of 16 mm diameter were obtained for receptors located at the fovea (Fig. 3A) and at three lateral regions (Fig. 3B–D). Color maps in Fig. 3 code the departure from the control r.m.s.LEOD. Black lines correspond to the limit determined by r.m.s.LEODs 2 s.d. apart from the control value in the absence of the object. In all cases the stimulus field is maximal when the sphere is in front of the recording point and rapidly decays when the sphere is moved a short distance away.

The spatial extensions of the stimulus field are maximal at the jaw–snout region (Fig. 3A,B). In order to depict a reference line, we overlapped the stimulus fields for each recording point and traced a smooth envelope line such that it encompassed the 2 s.d. lines obtained for each local recording point. For a steel sphere of 16 mm diameter, the maximal distances between the skin and the envelope line (black dashed lines overlapped on each stimulus field in Fig. 3) were 21.4, 22 and 20 mm; 10.2%, 11% and 9% of the fish's total length, respectively. This line was always less distant than 2 sphere diameters (N=3 fish). These results are compatible with those obtained by modeling and field measurements in other species (Rasnow, 1996; Nelson and MacIver, 1999; Rother et al., 2003; Chen et al., 2005).

Stimulus fields for a point on the receptor mosaic showed regions of the space where the object causes an increase of the LEOD and regions where the object causes a decrease of the LEOD. For example, when the recording probe is at the fovea, conductive spheres placed in front increase the r.m.s.LEOD (hot colors) but the same sphere placed near the opening of the opercula causes a reduction of the r.m.s.LEOD (cold colors). Large conductive spheres (11 and 16 mm, Fig. 3A,B and Fig. 4B,C) facing the peri-opercular region cause a massive draining of current, reducing the LEOD at the fovea. The same large sphere placed near the rostral pole increases the funneling effect, causing a LEOD reduction on the side of the fish (Fig. 3C,D).

The shape and extension of the stimulus field of a given point of the mosaic depend on its position along the fish. As the recording point was moved caudally, the stimulus field changed in shape as a result of the fish funneling effect (Castelló et al., 2000). For example, there were two separate regions in the stimulus field of a caudal location, a depressive 'horn' extending rostrally from the region adjacent to the head (Fig. 3D, sky blue) and an exciting core at the surroundings of the recording electrode (Fig. 3D, yellow–orange–red).

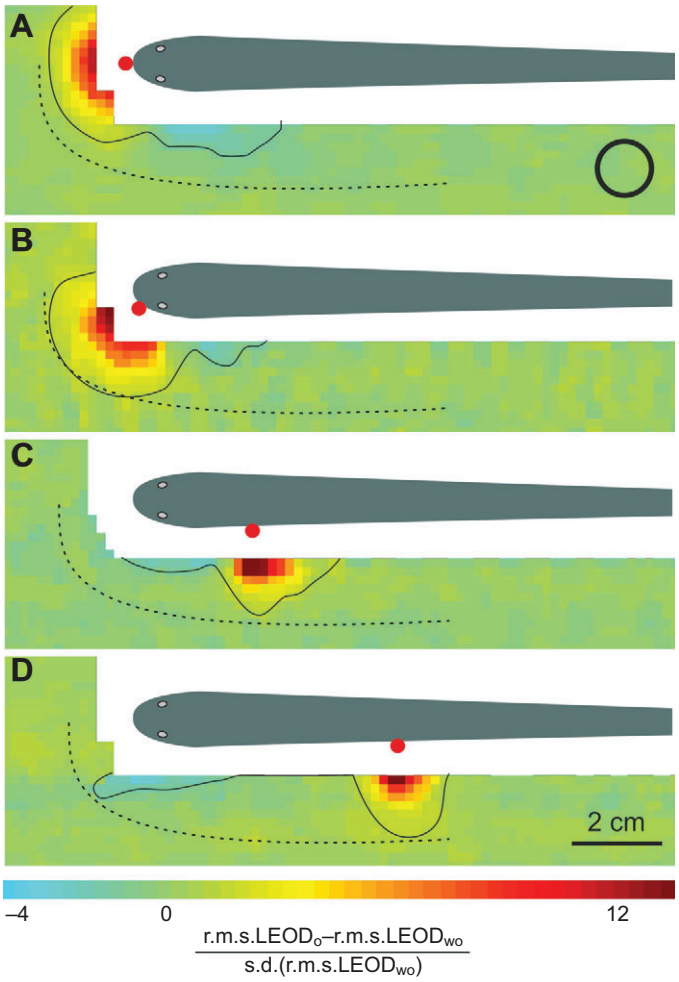

Fig. 3. The physical stimulus field at different points on the fish's skin. The figure compares the stimulus fields of four selected points on the skin (foveal region, A; and three lateral regions, B–D) explored by moving a sphere of 16 mm diameter. Each point in the map corresponds to a different position of the center of the sphere. Hot colors code for an increase and cold colors for a reduction of the stimulus at the recording point (marked by the red dot). The departure of the stimulus from the basal value is calibrated in standard deviations of the basal value (r.m.s.LEOD$_o$–r.m.s.LEOD$_{wo}$)/s.d.(r.m.s.LEOD$_{wo}$), where subscripts o and wo indicate the presence and absence of the object, respectively. The spatial extension of the stimulus field is greater in A and B (points at the foveal region or near it). In all cases maximal stimulus field occurred when the sphere was in front of the set of recording electrodes and it decayed significantly when the sphere was moved away. Green regions indicate no object effect. Black lines indicate the limit of the stimulus fields if they were sensed at 2 s.d. from the basal. The dotted line indicates the envelope of these lines. The circle indicates the size of the sphere.

The stimulus fields also depend on sphere diameter (Fig. 4). For small spheres (8 mm diameter, Fig. 4A), the 'Mexican hat' trough is less likely to be sensed as it is comparable to noise and in all cases is restricted to a small volume surrounding the recording point on the skin. It is important to note the extension of the stimulus field of the foveal region for relatively larger objects. For a 16mm steel sphere it clearly encompasses a volume surrounding the head and part of the rostral trunk (Fig. 4C).

The amplitude of the r.m.s.LEOD decayed with distance following monotonic functions when the sphere is moved away along a line perpendicular to the skin. This point is illustrated in

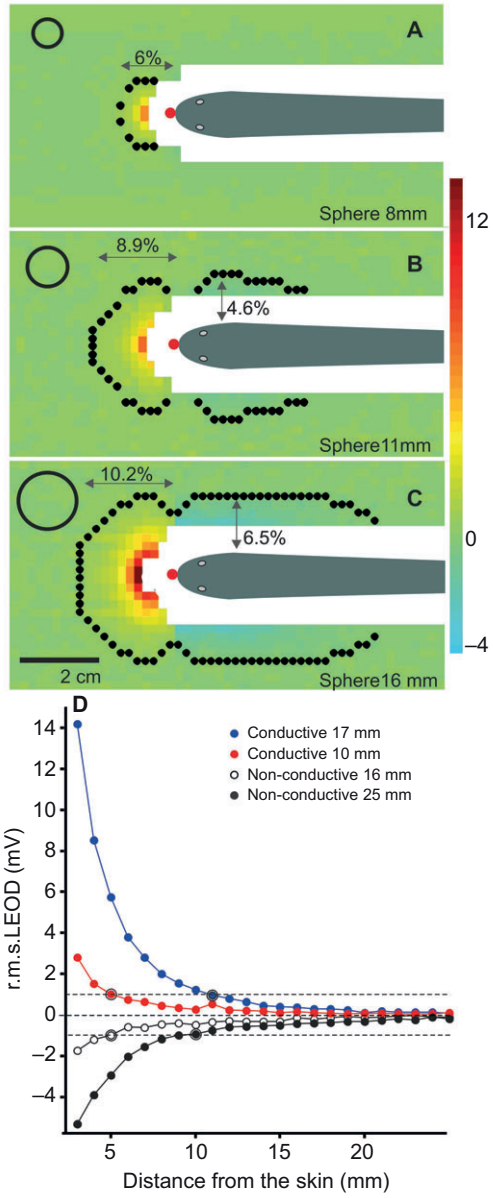

Fig. 4. Effect of object size and conductance on the stimulus field. (A–C) Color maps show the stimulus fields of the fovea explored with metallic spheres of different diameters. Each point in the map corresponds to a different position of the center of the sphere. Hot colors code for an increase and cold colors for a reduction of the stimulus at the fovea (marked by the red dot). The departure of the stimulus from the basal value is calibrated in standard deviations of the basal value (r.m.s.LEOD$_o$–r.m.s.LEOD$_{wo}$)/s.d.(r.m.s.LEOD$_{wo}$). Note that the range increases with object diameter (black dots indicate the 2 s.d. border positions corresponding to about 6, 9 and 10% of the fish's total length for spheres of 8, 11 and 16 mm, respectively; the circles encode the sizes of the spheres). (D) The departure of the local field from the basal field in the absence of objects as a function of the distance of a sphere placed at different points along the main axis of the body. Images of spheres of different size and conductance were obtained from the same fish. The dashed lines indicate the absolute value of the departure from the basal line. The distance required to stimulate the skin with this amplitude using a 10 mm sphere is duplicated by a conductive sphere of 17 mm (encircled points). A similar difference occurs for non-conductive spheres of 16 and 25 mm diameter (encircled points). Note that for a given LEOD departure from the basal, the distances required by conductive spheres are longer than those required by non-conductive spheres of similar diameter.

Fig. 4D, which compares the decays of the images of steel and glass spheres at the fovea (sphere diameters 10–25 mm). As expected, conductive spheres have a much larger effect than non-conductive spheres of similar size (Fig. 4D, compare blue and white dots). Increments in size compensate for this difference in conductance (Fig. 4D, compare the encircled dots in red conductive 10 mm and white non-conductive 16 mm plots).

These results suggest that: (a) for small objects, the stimulus field of a given point is an ovoid-shaped volume around this point; (b) for large objects, the stimulus field increases in volume having preferential extensions at the rostral pole and the gill openings (see Fig. 3D, Fig. 4A); (c) the range of active electrolocation increases with object size; and (d) for edible prey this range is likely much less than a fish's length.

Physical basis of image amplitude decay with distance

To test the theoretical prediction of the double influence of distance, we designed experiments in which the object was placed at different distances and we measured the resulting object stamp from the polarization of the object by the EOD or the transcutaneous field caused by a source connected to the poles of the object. To estimate the object stamp we calculated the parameters of the Thevenin equivalent of a scene 'electrically viewed' from an object placed at a given distance. We recorded the drop of voltage (V_o) across different objects' loading resistors (R_o). We estimated the current passing through the object using Ohm's law ($I_o=V_o/R_o$). In these experimental conditions we confirmed that V_o is a linear function of I_o (Fig. 5A, Eqn 3).

The Thevenin equivalent of the scene electrically viewed from each object position was characterized by two parameters that were easily estimated from the fitting lines (Fig. 5A): electromotive force (E_s, ordinate intersects) and series resistance (R_s, slopes). We found that E_s monotonically decayed with distance. R_s increased with distance within a range of a few millimeters from the skin (Fig. 5A, compare red and black lines). Beyond this distance R_s was nearly constant (Fig. 5A, compare the slopes 'seen' from the point of view of the object).

In the close neighborhood of the fish, the presence of a highly conductive fish's body reduces R_s with the net result of a slow decay in the absolute value of the stamp (Fig. 5B). We verified that R_s is an increasing function of distance (P=0.016, Wilcoxon sign-rank test, N=6). When the object moved towards the fish the graph shows an abrupt reduction of R_s (Fig. 5B). In addition, the electromotive force shows a departure from the power law (Fig. 5C, sky blue area). This departure is probably the consequence of the interaction between the fish and the object. The object-perturbing field causes a new stamp of the fish's body and this, in turn, projects again on the object. This interaction increases with the reduction of the distance between the fish and the object (Fig. 5C). These two phenomena are the basis of a third distance effect on active electrolocation.

Far from the fish, in the absence of close boundaries or other objects, R_s is nearly constant, and so I_o is proportional to E_s. The field generated by the fish decays with distance following a power law; thus, E_s and S decay in the same way for the same object characteristics,

Fig. 6A,C (blue dots) shows in a log–log plot that for distances longer than 4 mm, the stamp (S) follows a decreasing power function of distance (d) with a decay exponent α:

$$S = k_1 d^{-\alpha}, \quad (7)$$

where k_1 is a constant depending on the fish.

It is important to note that the points close to the fish (encircled point in Fig. 6A) depart from the fitting line. This is due to the interaction between the object and the conductive body occurring within a fringe of a few millimeters from the skin. When the object moves beyond this fringe this effect disappears and the slope of the function increases.

Decay in object polarization is not the only factor that determines image decay with distance. The modulation of the field caused by the presence of the object can be considered as the electric field generated by the object's stamp (object-perturbing field) (Lissmann and Machin, 1958). This electric field generated by the stamp also decays with distance, following similar laws to a field generated by

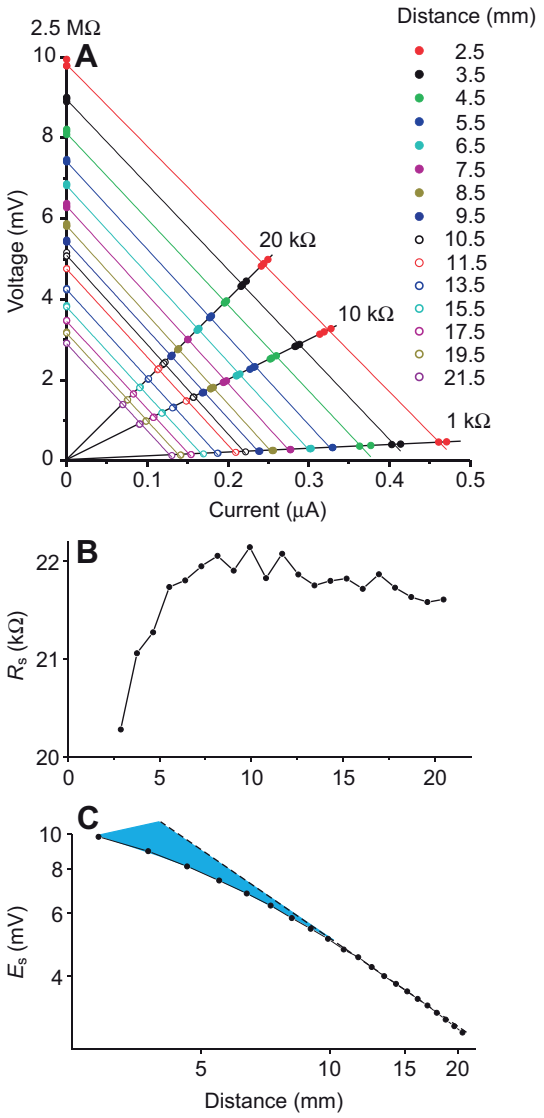

Fig. 5. Theoretical analysis of the physical problem and parameter measurements. (A) Each graph corresponds to an experiment performed at a given distance (see color code in the key). Each point of the graph indicates the drop of the r.m.s. voltage across and the r.m.s. current through the object probe (voltage divided by resistance) when the carbon base was connected by a given resistor (1 kΩ, 10 kΩ, 20 kΩ and 2.5 MΩ). For each distance, the electromotive force of the scene from the point of view of the object (E_s) was calculated as the ordinate intercept of the fitting line. The scene resistances from the point of view of the object (R_s) are represented by the slopes of the fitting lines. Scene resistance (B) and electromotive force (C) of the scene 'seen' from the point of view of the object are plotted as functions of distance between the fish and the object. For further explanation, see Materials and methods and Results.

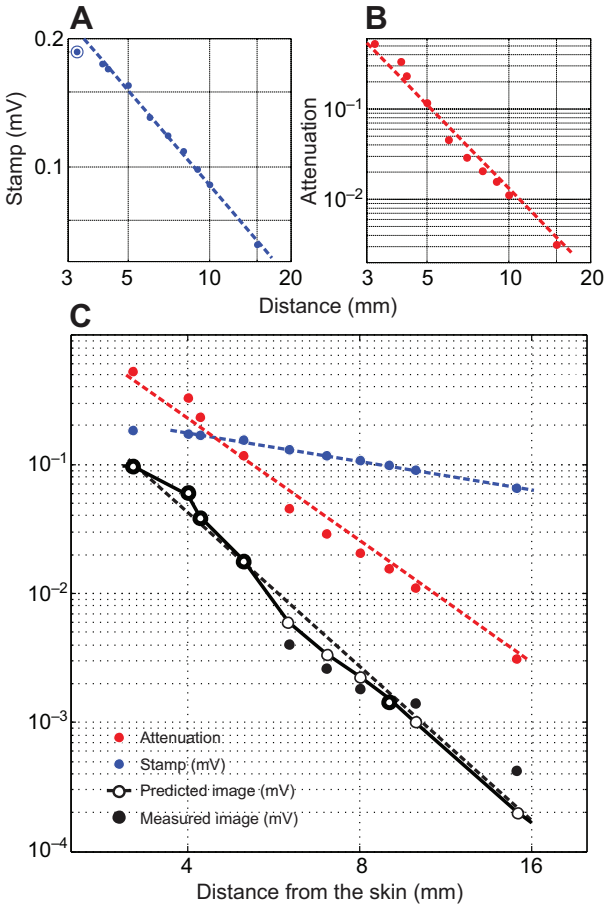

Fig. 6. Experimental measurements confirm the double attenuation mechanism. (A) A log–log plot of a cylindrical object stamp as a function of distance (slope α=0.8). Note the departure of the object's stamp from the straight line (power law) at a short distance from the skin. This slope value depends on object dimensions (in this case we used a 2 mm diameter, 18 mm length cylinder). The procedure for constructing this graph is explained in Fig. 5 and in Materials and methods. (B) A log–log plot of object-perturbing field attenuation as a function of distance between the fish and an electric source (slope β=3.0). To construct this plot we measured the r.m.s.LEOD while clamping the voltage between the top and bottom of the cylindrical object with a sine wave of 400 mV peak to peak. We calculated the external stamp (S_e, see Eqn 5) as the applied r.m.s. voltage multiplied by the resistance of the water displaced by the object (R_w) over the scene resistance 'seen' by the object (R_s). Attenuation was calculated as the quotient r.m.s.LEOD divided by S_e (see Eqn 6). (C) Superimposed log–log plots show the object's stamp (blue dots), the external source-perturbing field (red dots) and the recorded image (black dots) as a function of object distance. The dashed line was calculated theoretically as the addition of α and β (3.8). The white dots linked by a continuous line correspond to the predicted image calculated for each point as the product of the recorded stamp and attenuation.

a dipole equally placed. We were able to measure this decay by clamping the voltage at the ends of the object and measuring the juxta-cutaneous field (JCF) at the center of the fovea for each object position. Attenuation (A) was defined as in Eqn 6.

Fig. 6B,C (red dots) shows in a log–log plot that for distances larger than 4 mm the attenuation follows a decreasing power function of distance and is proportional to the stamp of the source applied to the object. The slope of the line is the decay exponent (β). The proportionality constant (k_2) depends on the experimental conditions (tank, fish size and water conductance). When the

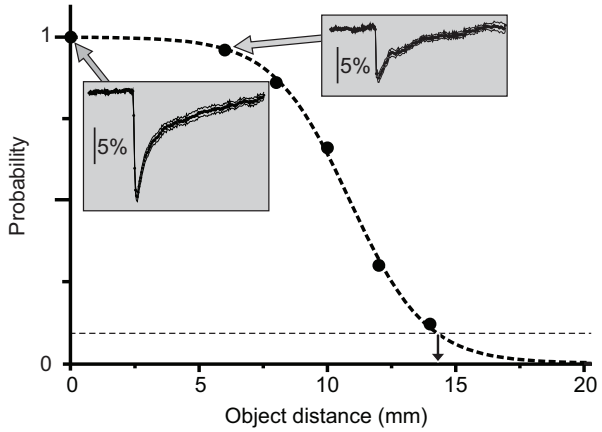

Fig. 7. The active electrolocation range. Estimated probability of the novelty response is plotted as a function of object distance. The active electrosensory limit was determined as the abscissa of the point where the fitted sigmoidal curve crossed a reference threshold (0.1). The insets compare the amplitudes of novelty responses at two different distances where they occur in 100% of the trials (relative frequency=100% corresponds to probability=1).

object-perturbing field is generated by the stamp of the object the image follows the same power rule:

$$\text{Image} = Sk_2d^{-\beta} . \quad (8)$$

This reasoning implies that beyond 4 mm, the image decays as the product of both factors (Fig. 6C, black dashed line), explaining the very important attenuation of the image verified experimentally (Fig. 6C, black dots). As a comparison we calculated the image from the product of stamp and attenuation and overlaid the plot with the measured data (Fig. 6C, white dots linked by a continuous line):

$$\text{Image} = k_1k_2d^{-(\alpha+\beta)} . \quad (9)$$

These results provide strong support to the double distance theory. We showed that, as expected from the theory, the stamp depends on the difference between the resistance of the water and the object and decays with a power law. The stamp effect is, in turn, further attenuated by another power function determining the short range of active electrolocation.

These results also show that there is a third distance-dependent factor next to the skin. This is due to the interaction between the fish and the object and was analyzed by modeling studies in mormyrid fish (Migliaro et al., 2005). In addition to the effect of fish body conductance, the distribution of the sources along the fish may also contribute to the observed departure from the power law (Caputi et al., 1989; Caputi and Budelli, 1995; Chen et al., 2005).

Behavioral assessment of the active electroreception range

To address object detection, we identified the novelty responses evoked by a change from 2.5 MΩ to 1 kΩ in the longitudinal resistance of a cylindrical object at different distances from the skin. We estimated the probability of the novelty response as the relative frequency defined as the number of identified responses expressed as a percentage of the number of trials. We found that the raster plots of the increments of the second-order intervals (ΔI^{2nd}) were more informative than the first intervals because a novelty response implies a sudden acceleration involving a few consecutive reductions of the interval. ROC analysis of ΔI^{2nd} indicated that the critical value of the probability of novelty

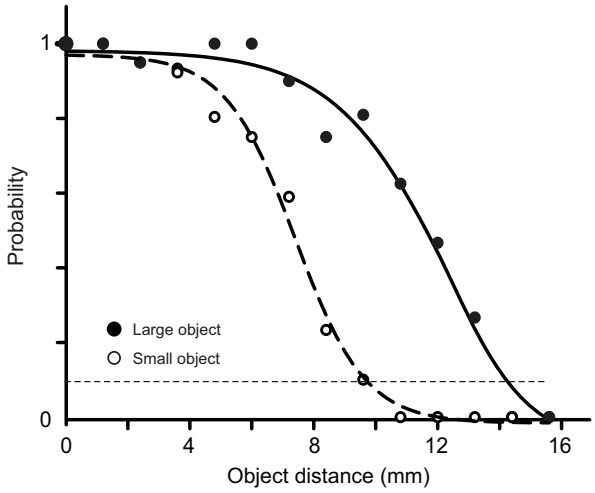

Fig. 8. Effect of object size on the active electroreception range. Probability of the novelty response (estimated by the relative frequency defined as the number of identified responses expressed as a percentage of the number of trials) as a function of distance for two cylindrical probes. Small object: 6 mm diameter, 12 mm length. Large object: 8 mm diameter, 20 mm length.

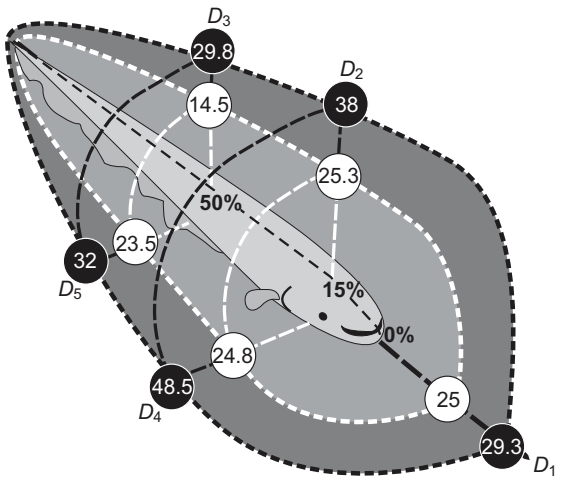

Fig. 9. Active electrolocation bubble. (A) Summary of the results obtained from four fish using cylinders of 6 mm diameter and 12 mm length (small object; white circles and white dashed lines) and 8 mm diameter and 20 mm length (large object; black circles and black dashed lines). Range is indicated for each explored direction as the median distance in mm from the skin (N=4).

responses to address object detection using visual inspection of the rasters was 0.1 (see Appendix).

In a first series of experiments we evaluated the active electrosensory range for cylindrical probes of 6 mm diameter and 12 mm length. We plotted the probability of the novelty response as a function of the object distance and fitted the data with a sigmoidal curve (Fig. 7). We evaluated the active electrolocation range by determining the distance at which the relative frequency of the novelty response was equal to or smaller than 10% according to the fitted curve (Fig. 7, arrows). Note that in the region where the novelty response always occurs, its amplitude also decays with distance (Fig. 7, insets).

Physical measurements suggested that the active electrosensory detection range was longer for larger objects. One must recall that the stamp of our probes depends on the difference between the imposed resistance and the longitudinal resistance of a displaced cylinder of water (R_w) and also on the value of the strength of the polarizing field determined by the object length (Pereira and Caputi, 2010; Aguilera et al., 2012). As we used a maximal change in resistance of the object probe, from 2.5 MΩ to 1 kΩ, we compared the effect of object length by paired experiments using probes displacing cylinders of water of the same longitudinal resistance. A Wilcoxon sign-rank test indicates that the active electrolocation range is longer for longer objects aligned in the same way to the field (P=0.0004, N=20 pairs of experiments). The sigmoidal function relating probability of the novelty response and distance is shifted to the right for longer objects (Fig. 8, see also ROC curves in Appendix).

Table 1 and Fig. 9 compare the results obtained with large (8 mm diameter, 20 mm length) and small (6 mm diameter, 12 mm length) objects in the same four fish along the five explored directions. In addition to the clear differences between large and small objects, inspection of Table 1 suggests the possibility of preferred directions. For small objects there is a slightly shorter detection range when the

Table 1. Statistics of the active electrolocation range in five directions

	Detection range parameter	Exploring direction				
		D_1	D_2	D_3	D_4	D_5
Small object	Mean	25.3	27.9	14.8	25.1	23.5
	s.d.	7.0	8.4	1.0	3.4	5.4
	Minimum	18.0	21.0	14.0	22.0	17.0
	Median	25.0	25.3	14.5	24.8	23.5
	Maximum	32.5	40.0	16.0	29.0	30.0
Large object	Mean	28.1	38.5	30.9	47.2	34.8
	s.d.	7.5	6.6	15.3	14.5	10.1
	Minimum	19.0	32.0	15.0	32.0	26.5
	Median	29.3	38.0	29.8	48.5	32.0
	Maximum	35.0	46.0	49.0	61.0	46.0
Large/small	Median ratio	1.17	1.50	2.06	1.96	1.36

Range measurements (mm) were performed in the same four fish using two test objects: small, 8 mm diameter, 20 mm length; large, 8 mm diameter, 20 mm length.

D_1, rostral, along the midline; D_2, up from the top of the head; D_3, up from the middle; D_4, sideways from the gills; D_5, sideways from the middle.

N=4 fish.

object faces the dorsal aspect at the middle of the fish's body length (direction D_3). A Kruskall–Wallis test comparing median detection ranges for five different directions for the small object showed a low probability of uniformity (P=0.0379, d.f.: columns 4, error 15). *Post hoc* analysis excluding direction D_3 indicated uniformity among others (P=0.68, d.f.: columns 3, error 12) and a Wilcoxon rank-sum test comparing the dorsal direction (N=4) with the pooled rest (N=16) indicated clear differences in the median (P=0.002). Thus, for small objects in front of the caudal region, the range might be shorter than for other object locations. For large objects a Kruskall–Wallis test suggested no preferred directions (P=0.1, d.f.: columns 4, error 15). This indicates a different 'shape' of the electrodetection bubbles. The ratio between the median detection distances along each direction confirms this hypothesis (Table 1). Interestingly, the smallest ratio is along the mean axis of the fish because of the more pronounced decay of the field along direction D_1.

To address the question of whether acuity decreases with distance faster than detection, we explored the probability of a novelty response evoked by a 'virtual change in object position' as a function of distance. We simulated an object movement along a line parallel to the fish by simultaneously shunting and disconnecting two pairs of electrodes placed on each side of the midline and at the same distance from the skin (see Materials and methods). In these conditions the images are similar but located on opposite sides of the fish.

Novelty responses evoked by 'object virtual movement' were evoked very consistently (97±3% of the runs, N=6) when the closer electrodes were almost in contact with the skin. Data from five fish show that the probability of the novelty response evoked by the virtual movement of a virtual object drops from 98% to 36% (median values) when the probe is moved from a juxta-cutaneous position to 5 mm away (Wilcoxon sign-rank test, P=0.032, N=5). In addition, a sign-rank test showed that the probability of the novelty response caused by an object 'movement' was significantly smaller than the 'appearance' of an object at the same site (P=0.016, N=6, 5 mm distance).

To isolate this result we explored the decay of probability with distance of the virtually moving object (Fig. 10). The relative frequency of novelty responses was reduced following a sigmoidal curve, dropping below 10% of the trials at 9 and 12 mm, respectively, in two fish (the corresponding controls for shunting a single pair were 75 and 35%). These results suggest that *G. omarorum* is able to precisely locate an object at a distance shorter than the critical distance for detecting it.

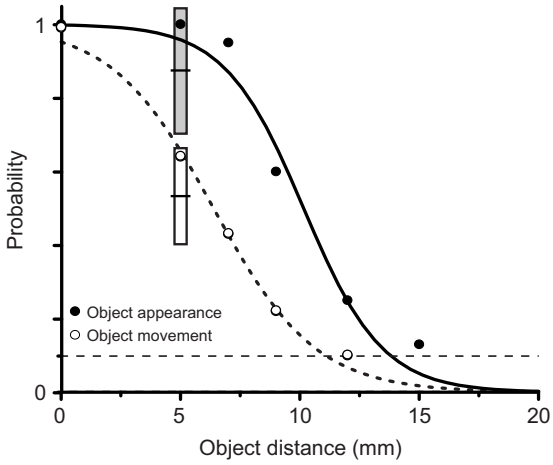

Fig. 10. Electrolocation precision vanishes at short distances. Estimated probability of the novelty response plotted as a function of the distance of the probe used for mimicking object movement (open symbols). The probe consisted of two pairs of electrodes symmetrically placed on each side of the midline. Right and left electrodes were alternately shunted by a 1 kΩ resistor to mimic a change in position of the object from one side of the midline to the other (the experiment started with the right pair of electrodes shunted and the stimulus consisted of the simultaneous disconnection of this pair and the connection of the left pair). The dashed line indicates a 0.1 probability threshold criterion. Filled symbols indicate the probability of the novelty response when only one pair of electrodes was shunted. Boxes and lines (ranges and the median values) compare the probabilities evoked by the 'appearance' of the object (gray) *versus* the 'movement' of the object (white) obtained from N=6 fish at 5 mm distance. The horizontal dashed line indicates the median value of these experiments (Wilcoxon sign-rank test, P=0.017).

DISCUSSION

Active electroreception is generally involved in the location of objects and navigation. Both tasks require, besides a precise internal representation of the external space, the possibility of identifying reference clues from a certain distance. We found that active electroreception is not suitable for detecting invariant reference clues beyond few centimeters from the skin in *G. omarorum*. Although this precludes navigation under the sole guidance of this sensory modality, the fish might memorize a path as an orderly series of sensory events (Burt de Perera, 2004). Here, we reported physical and behavioral experiments confirming that the short active electrolocation range is similar to that obtained in *Apteronotus* (MacIver, 2001; Nelson and MacIver, 1999; MacIver et al., 2001). Taking into account the fact that the EOD of pulse mormyrids is six times larger in electromotive force, their normalized active electroreception range is also similar to that reported here (Heiligenberg, 1976; Push and Moller, 1979).

Object distance and its consequences for electroreception

We experimentally tested that the transcutaneous field (LEOD) in the presence of an object can be calculated as the sum of the basal LEOD in the absence of an object plus the perturbing field generated by the presence of the object. This hypothesis leads to the explanation of the short active electrosensory range of these fish. The double distance theory, whose conceptual evolution is addressed in the Introduction, implies that there are two mechanisms by which the electric image decays when the object is moved away: (1) object polarization decays with distance from the fish to the object; and (2) the perturbing field also decays with the distance from the object to the fish.

For a simple scene, each of these decaying functions follows power laws, with their exponents depending in a different way on the distance to the borders of the tank and the fish (Chen et al., 2005; Pereira and Caputi, 2010). As the amplitude of the image results from the product of the attenuation functions by object polarization and object-perturbing fields, the power law ruling the attenuation of the image with distance is characterized by the sum of such exponents. Simultaneous measurement of the stamp and the image of objects confirmed this multiplicative effect (Fig. 6).

A third mechanism is evident when one analyzes more real, complex scenes. Other objects may extend or reduce the range of detection of an object of interest because of mutual polarization of nearby objects (Aguilera et al., 2012). This also explains the effects of the tank walls and the deepness of the water.

It is important to note the differences in the attenuation profiles found for the object-perturbing field and the object's stamp. The conductive fish's body causes a reduction of the scene equivalent

resistance as seen from the point of view of the object (R_S) (Pereira and Caputi, 2010). As a consequence, within a narrow juxta-cutaneous fringe, the stamp of the object attenuates less with distance. This led us to conclude that by this third important mechanism the distance between the object and the fish is crucial for determining the perceptual characteristics of the object. Only within a juxta-cutaneous fringe caused by the interaction between the object and the fish's body are the details of object surface (Caputi et al., 2011) and object location precisely sensed. Our experimental findings not only confirm previous theoretical predictions indicating that the signal attenuation is reduced in the vicinity of the skin (Migliaro et al., 2005; Chen et al., 2005) but also show the importance of the high conductance of the fish's body (Migliaro et al., 2005; Pereira and Caputi, 2010) and support our previous explanation of why very sharp images of the object surface are only possible within a juxta-cutaneous fringe (Caputi et al., 2011).

The stimulus fields and their variation for different points of the receptive mosaic

Consistent with previous data (Rasnow, 1996; Chen et al., 2005), our experiments show that the stimulus field increases with sphere diameter. Spheres of greater diameter shunt (or block) the current across equivalent longer distances, causing stamps of larger absolute values. As the drop of voltage at the object site must be attenuated up to the same r.m.s.LEOD, spheres of larger diameter are detected at longer distances. One of the aspects of this observation is illustrated by the encircled points of Fig. 4: a 10 mm conductive sphere placed at 5 mm from the skin generates the same change in r.m.s.LEOD (1 mV) as a 17 mm conductive sphere placed at 11 mm. The stimulus fields of larger objects cover a larger volume (Fig. 4, color maps). Because of the hyperbolic relationship between the stamp and the object impedance (Eqn 4), non-conductive spheres have less effect for the same diameter; for example, a non-conductive sphere of 16 mm diameter generates the same effect as a conductive one of 10 mm.

The other aspect is that the fish body acts as a 'fast-track path' for the electric field and also the tapered shape of the fish's tail funnels the field from caudal to rostral regions (Caputi and Budelli, 1995; Aguilera et al., 2001). This has two effects: one is that in the vicinity of the head the object will be differently polarized; the other is that the distance necessary to attenuate the same stamp will be different for different positions of the object.

Considering a source oriented towards a recording point in open water, the attenuation distance will be the same for all directions; thus, the stimulus field of such a point will be a sphere. When this point is on the skin of a fish, the conductive body will extend the detection distance along a direction parallel to the skin. Thus, for objects of small size compared with the skin curvature the stimulus field is elongated, acquiring an oval shape. Large objects close to the fish may increase or decrease the funneling effect; thus, the object would cause increments of current flow across a local region of the skin large enough to generate distant opposite effects because of the Gauss theorem (Sears and Zemanski, 1955).

This theoretical reasoning was confirmed by our recordings: small spheres had a local effect and an oval-shaped stimulus field. However, large spheres are able to stimulate the fish with the same intensities from longer distances and show extended stimulus fields of elongated shapes.

Although the foveal region is small, it has a relatively large stimulus field because of the funneling effect (Castelló et al., 2000). It serves the fish not only for detailed exploration of objects (Caputi et al., 2011) but also to detect them in the surroundings of the head region. For example, the stimulus of foveal receptors increased beyond 2 s.d. of the mean basal amplitude when a 16 mm diameter steel sphere was located rostral to the fish up to 20 cm away along the midline. Interestingly, these spheres caused a reduction of the stimulus at the fovea when they were placed at the level of the rostral trunk. This is probably due to a large draining of current in front of the object and also through the gills. This suggests that the foveal region (where electroreceptor density is maximal) has a large stimulus field, including a region facing the rostral trunk.

For electroreceptors on the middle of the trunk, large steel spheres caused a strong increase of the LEOD when they were in front of it, but also caused a distant effect consisting of a reduction of the LEOD when they were close to the head. This last effect is probably due to the increase in the funneling effect.

Behavioral evidence for short detection range and the decay of location precision

The active electrosensory range shown by behavioral responses matched that of physical measurements. Comparing the stimulus field with the electrolocation range estimated using the novelty response, we may roughly estimate that fish detect departure from the basal field ranging between 1 and 2 s.d. Combining data from mormyrids (Heiligenberg, 1976; Push and Moller, 1979), wave gymnotids (Nelson and MacIver, 1999) and the pulse gymnotids reported here, one can conclude that they are similar, and in consequence active electrolocation is a short-range sensory modality.

Behavioral estimation of the active electrolocation range was on average less than one-fifth of the fish's total length and never surpassed one-third for any of the experiments reported in this study. On the side of the fish, distance increased by a factor of 1.39 in accordance with other data in the literature (Heiligenberg, 1975; Heiligenberg, 1976). In *Brienomyrus*, the detection range increases with the square root of object diameter (Heiligenberg, 1976); thus, a doubling of object diameter should correspond to an increase of the range by a factor of 1.41.

As predicted by physical measurements, the effect of doubling object size is not the same when the object is in different positions with respect to the fish. While the range increases by a small factor (1.17) at the rostral pole, it doubles when the object is in front of the gills (Table 1, Fig. 9). It is important to note that the longitudinal resistance of the large and small objects was similar because they were constructed in such a way that longitudinal resistance of the displaced water cylinders was similar. Therefore, among cylinder characteristics, length was the only significant variable to determine our probe stamp. Distances were measured from the closest point of the objects; thus, they were underestimated for longer objects (4 mm). This implies that the stamp was further reduced in the case of longer objects. In spite of this handicap in the comparison, longer objects were always sensed at a longer range. In addition, the stamp of the object is dependent on the drop of voltage across the displaced water cylinder. Because of the convexity of the field, the stamp of a short object better follows the local field and the stamp of a large object reaching regions where the potential is negligible better follows the basal potential at the distance from the fish at which its rostral face is placed. The steepest decay of the field along the main axis near the fovea explains the small ratio between detection distances corresponding to large and small objects.

One may speculate that the effect of very large objects may be observed from relatively longer distances, opening the possibility of detecting floor, water surface, walls and relatively large objects that may serve as relatively fixed cues. This was clearly shown in

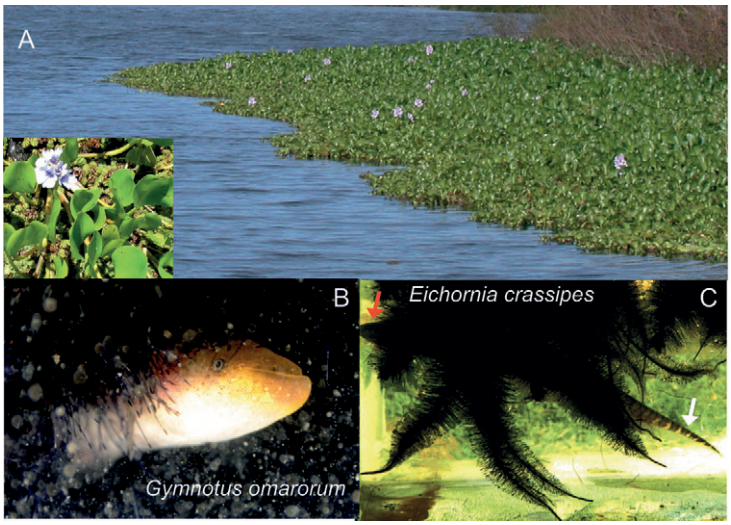

Fig. 11. *Gymnotus* habitat. (A) Panoramic photograph of an island of floating plants in Laguna del Cisne, Maldonado, Uruguay (34°49′31.03″S; 55°03′37.31″W). Inset: large leaves and flower of *Eichornia crassipes*. Note the presence of other small plants in this case. (B) *Gymnotus omarorum* hiding within the roots of *E. crassipes*. (C) The roots of *E. crassipes* have a very soft and flexible brush-like structure. Note the fish profile (head red arrow, tail white arrow).

Apteronotus (Chen et al., 2005) and also in artificial electrosensoy artifacts (MacIver et al., 2004; Boyer et al., 2011). However, image spread with distance and sensory adaptation makes this mechanism only useful for defining a rough course that is continuously adjusted. In fact, our experimental data showed that electric images of an object may be indistinguishable from those of another object placed several millimeters on its side as their distance to the skin increases. A 'virtual movement' occurring as close as 5 mm away causes novelty responses in only 66% of the runs on average. At the same distance the same object is much more frequently detected, indicating that the absence of a response to image movement on the receptor mosaic is not due to the absence of a detectable image (Fig. 10). This lack of difference between images of two objects placed close together, but at a certain distance from the fish, results from the fact that electric images are superposition images (Rasnow, 1996; Caputi et al., 1998; Sicardi et al., 2000; Pereira and Caputi, 2010). Thus, images of two objects far from the fish are sensed as being equal because of their increase in width.

What is the most probable use of active electroreception in the natural habitat?

Our analysis suggests that navigation using active electric sense is similar to vision-based navigation in a dense fog. We have previously shown that active electroreception in pulse gymnotids uses the fish's body to sense in detail the space adjacent to its body (Caputi et al., 2011). Here, we have shown that they have a short electrosensory range and that they have a coarse sense of position of relatively close objects. Teleceptive senses such as vision, hearing or the sense of gravity detect signals generated far enough from the subject so that their presence immediately evokes an allocentric reference framework for conceiving the external world and navigating in it. Senses such as touch detect signals generated close to the animal but, more importantly, as they are active, they should be referred to an egocentric spatial framework. While teleceptive senses require only a few relatively fixed clues for navigation and locating objects within a reference space, haptic senses such as active touch and electrolocation, lacking the possibility of finding fixed references once the animal has moved, require tracking clues that link previous and present sensory images (Burt de Perera, 2004).

As for other electric fish (Snyder et al., 2007), *G. omarorum* has a body-centered active electrosensory bubble that follows the fish's movements and probably body bending (Fig. 9). In *Apteronotus*, active electrosensory and skeletomotor bubbles match well, as predicted by modeling and confirmed by experimental studies (Snyder et al., 2007; MacIver et al., 2010). Because of the similarity between the skeletomotor strategies and the similarities found in active electrosensory range, it is likely that the same matching holds for *G. omarorum*. This indicates that gymnotiforms may easily stop to avoid an obstacle or efficiently track an object when it is inside the electrosensory–skeletomotor bubble (Snyder et al., 2007; MacIver et al., 2010). However, they should not be able to find defined active electrosensory clues beyond a range equivalent to the fish's length. In fact, our data indicate that the *G. omarorum* detection range is, at the most, three object lengths and that they are not able to precisely discriminate the location of a relatively large object beyond 1 cm. As a consequence, it is doubtful whether the electric sense is involved in long-range navigation tasks except for tracking external electric fields generated by other conspecifics. This speculation is also consistent with the data of Hopkins and his collaborators (Schluger and Hopkins, 1987; Davis and Hopkins, 1988) who have shown that electronavigation is supported by passive electrolocation (a sensory modality having a longer range than active electrolocation), which requires the presence of electric fields as a reference clue. The fish follows field lines and once the field is suppressed electronavigation is severely impaired.

Our own data from the field (A.A.C., unpublished observations) indicate that *G. omarorum* is a lonely animal usually found about 1 m away from conspecifics. *Gymnotus omarorum* are very territorial and aggressive animals (Black-Cleworth, 1970; Batista et al., 2012) living camouflaged under the roots of water plants forming floating islands in shallow waters (*E. crassipes*, Fig. 11A). The roots of these plants are soft feather-like structures forming a labyrinth (Fig. 11B,C) in which the fish has to find prey without the help of vision. Thus, for this sponge-like environment an electric carrier propagating through water between the root filaments appears to be an optimal adaptation. While plant islands may move many kilometers under the effects of the wind, *G. omarorum* appears to be adapted to move with them, having its ecological niche as a reference no matter where it is in relation to static geographical landmarks. Therefore, rather than distant object location and navigation based on fixed landmarks, it is probable that the main use of this active sense is for recognizing the contrast between the impedance of small potential prey and 'home cues' defined by the background patterns of impedance determined by a crowded maze of roots.

APPENDIX

Probability of novelty responses as an estimator of object detection

In previous articles we have used the novelty response as a behavioral indicator of a change in object impedance. We used two parameters, amplitude and probability. However, defining a threshold for detection posed us a general problem usually solved by using the signal detection theory (Green and Swets, 1966). The ROC consists of a plot of the cumulative probability of true positive detections *versus* the cumulative probability of the false-positive detections.

To construct the ROC we considered the series of increments in the second-order intervals. Novelty responses are generally characterized by a consecutive reduction of two or three intervals (Fig. 2A, top trace). Thus, when two consecutive intervals are significantly reduced, the sum of their increment shows a much larger reduction than the sum of changes of any other consecutive pair of intervals (the cancellation of an increment with the next one of opposite sign is the most common rule, Fig. 2A).

For each threshold level and run, true and false responses were classified as positive or negative. True positive responses were those negative ΔI^{2nd} that were under the threshold just after the stimulus (Fig. 2A, black and blue). False positive responses were those negative ΔI^{2nd} that were under the threshold between 30 and 25 EODs before the stimulus. Negative responses were those negative ΔI^{2nd} that were not under the threshold. The probabilities of true positive and false positive responses were functions of the chosen threshold (Fig. A1A). These functions were estimated in the following way. First, for each run we looked for negative increments of the second-order interval (ΔI^{2nd}) within a pre-defined 5 EOD window around (true responses) or 30 EOD before (false responses) the stimulus. Second, we defined a threshold and counted the number of ΔI^{2nd} that were under this threshold for the series of trials performed at such a distance and divided each count by the number of trials. Third, after repeating the procedure against a high enough number of thresholds (minimum 5) we plotted the cumulative probability of true (Fig. A1A, white bars) and false (Fig. A1A, black bars) positive responses as a function of the threshold value. Finally, for each distance, we constructed a ROC in which each point was determined by the pair of numbers corresponding to the cumulative probabilities of false (abscissa) and true (ordinate) positive responses obtained at the same threshold (Fig. A1B).

A quantitative way of measuring the significance of the departure from the identity of a ROC is the area between curves (ABC):

$$\mathrm{ABC} = \frac{\sum_k (\mathrm{fp}_k - \mathrm{fp}_{k-1}) \cdot (\mathrm{tp}_k + \mathrm{tp}_{k-1})}{2} - 0.5 , \qquad (A1)$$

where fp indicates false positives and tp indicates true positives. If detection is by chance, ROC overlaps the identity line. It is accepted that if ABC is larger than 10% of the total plot area detection, it is not by chance (Swets et al., 2000) (blue region of the plot in Fig. A1B). As an intuitive notion, an ABC equal to 0.1 means that when the threshold is set to detect 50% of the true responses one would have to accept the possibility of mistakenly accepting 35% of the false responses.

Close to the fish, true positives are detected at large threshold values. As a consequence they are well separated from the false positives, detected only at small threshold values. As most of the true positive responses are recruited before the false positive responses the corresponding dots lie on the left axis, and consequently the rest lie very close to the top axis. This determined a 'right-angle-shaped' ROC (Fig. A1B, orange dots). At intermediate distances the differences in the rate of increase of true and false positives with the decrease of the absolute value of the threshold determined the typical 'half-moon' shape of the ROC (Fig. A1B,

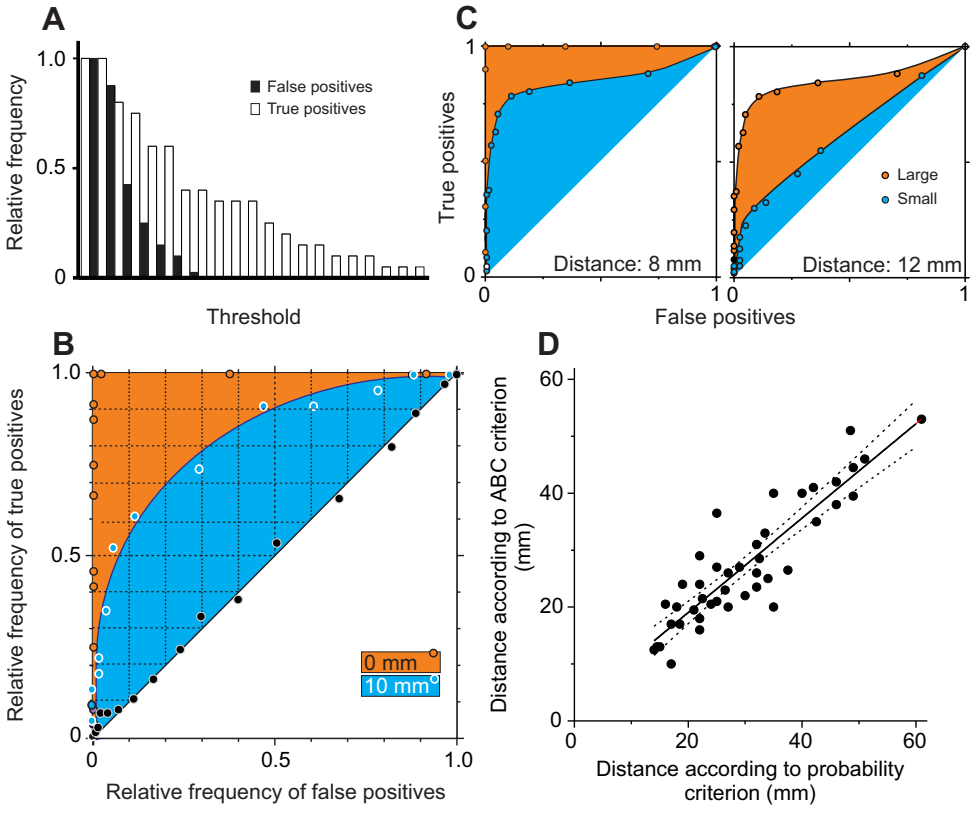

Fig. A1. ROC analysis. (A) Cumulative probability of false positive responses (black) and true positive responses as a function of the absolute value of threshold. (B) ROC curves for a juxta-cutaneous probe (orange), and for a probe at 10 mm (sky blue) and at 40 mm (black dots). A theoretical confidence limit encompassing areas between the curves below 0.1 is traced by the white line and shown in dark blue. (C) ROC curves for large (orange) and small objects (sky blue) at two distances. (D) Detection distance obtained using the ROC criterion *versus* detection distance obtained using the probability criterion (N=42, r=0.9, P<0.001).

blue dots and area). Finally, at far enough distances the ROC fell below the critical line because the probability of true and false positives became similar. The diagonal line obtained at 40 mm (Fig. A1B, black dots) was indistinguishable from the diagonal line obtained in controls that compared two false positive sets obtained either at 30 intervals before or 80 intervals after the stimulus (data not shown). The ROCs corresponding to the experiments performed with a short probe (Fig. A1C, blue dots and area) and a long probe (Fig. A1C, orange dots) placed at 8 mm (Fig. 1C, left plot) or 12 mm (Fig. 1C, right plot) from the fish illustrate that ROC departures from the identity line are larger for larger objects.

To validate the probability of visually identified novelty responses as a good detection criterion we constructed ROCs for 42 of the trials. For these experiments, we plotted the ABC as a function of distance (d), and fitted these plots with a Boltzmann-type sigmoid where k is the maximum slope and d_o is the distance that yields ABC=0.5:

$$ABC = \frac{1}{1 + e^{\frac{(d - d_o)}{k}}} \quad . \qquad \text{(A2)}$$

To evaluate the goodness of the probability criterion, we plotted the detection distance obtained using the ABC criterion as a function of the detection distance. We found that the distances for which the probability of a novelty response fell below 10% of the runs were well correlated to the distances obtained through ROC analysis. Fig. A1D shows the plot constructed from 42 of the experiments that gave rise to Table 1 (r=0.9, N=42).

ACKNOWLEDGEMENTS

We thank to Lic. M. Piffaretti for editing the English in an initial draft of the manuscript, Mr M. Lalinde for his help with the photography of the fish and the two anonymous referees whose comments helped to improve the final text.

FUNDING

This study was supported by European Commission Information, Society and Media Future and Emergent Technologies (FET) grant [no. 231845, PEDECIBA (Uruguay) and ANII (Uruguay)].

REFERENCES

Aguilera, P. A. and Caputi, A. A. (2003). Electroreception in *G. carapo*: detection of changes in waveform of the electrosensory signals. *J. Exp. Biol.* **206**, 989-998.
Aguilera, P. A., Castelló, M. E. and Caputi, A. A. (2001). Electroreception in *Gymnotus carapo*: differences between self-generated and conspecific-generated signal carriers. *J. Exp. Biol.* **204**, 185-198.
Aguilera, P. A., Pereira, A. C. and Caputi, A. A. (2012). Active electrolocation in pulse gymnotids: sensory consequences of objects' mutual polarization. *J. Exp. Biol.* **215**, 1533-1541.
Assad, C., Rasnow, B. and Stoddard, P. K. (1999). Electric organ discharges and electric images during electrolocation. *J. Exp. Biol.* **202**, 1185-1193.
Babineau, D., Longtin, A. and Lewis, J. E. (2006). Modeling the electric field of weakly electric fish. *J. Exp. Biol.* **209**, 3636-3651.
Bastian, J. (1981a). Electrolocation I. How the electroreceptors of *Apteronotus albifrons* code for moving objects and other electrical stimuli. *J. Comp. Physiol.* **144**, 465-479.
Bastian, J. (1981b). Electrolocation II. The effects of moving objects and other electrical stimuli on the activities of two categories of posterior lateral line lobe cells in *Apteronotus albifrons*. *J. Comp. Physiol.* **144**, 481-494.
Bastian, J. (1986). Electrolocation: behavior, anatomy and physiology. In *Electroreception* (ed. T. H. Bullock and W. Heiligenberg), pp. 577-612. New York, NY: Wiley.
Batista, G., Zubizarreta, L., Perrone, R. and Silva, A. (2012). Non-sex-biased dominance in a sexually monomorphic electric fish: fight structure and submissive electric signalling. *Ethology* **118**, 398-410.
Bennett, M. V. L. (1971). Electric organs. In *Fish Physiology*, Vol. V (ed. W. S. Hoar and D. J. Randall), pp. 347-491. London, UK: Academic Press.
Black-Cleworth, P. (1970). *The Role of Electrical Discharges in the Non-Reproductive Social Behaviour of Gymnotus carapo (Gymnotidae, Pisces)*, Vol. 3 of Animal Behaviour Monographs, pp. 1-77. London: Baillière, Tindall & Cassell.
Boyer, F., Gossiaux, P. B., Jawad, B., Lebastard, V. and Porez, M. (2011). Model for a sensor inspired by electric fish. *IEEE Transactions on Robotics* **28**, 492-505.
Budelli, R. and Caputi, A. A. (2000). The electric image in weakly electric fish: perception of objects of complex impedance. *J. Exp. Biol.* **203**, 481-492.
Bullock, T. H. and Heiligenberg, W. (ed.) (1986). *Electroreception*, 722 pp. New York, NY: Wiley.
Bullock, T. H., Hagiwara, S., Kusano, K. and Negishi, K. (1961). Evidence for a category of electroreceptors in the lateral line of gymnotid fishes. *Science* **134**, 1426-1427.
Caputi, A. A. (1999). The electric organ discharge of pulse gymnotiforms: the transformation of a simple impulse into a complex spatio-temporal electromotor pattern. *J. Exp. Biol.* **202**, 1229-1241.
Caputi, A. A. (2004). Contributions of electric fish to the understanding sensory processing by reafferent systems. *J. Physiol. Paris* **98**, 81-97.
Caputi, A. A. and Budelli, R. (1993). A realistic model of the electric organ discharge (EOD) of *Gymnotus carapo*. *J. Comp. Physiol. A* **173**, 751.
Caputi, A. A. and Budelli, R. (1995). The electric image in weakly electric fish: I. A data-based model of waveform generation in *Gymnotus carapo*. *J. Comput. Neurosci.* **2**, 131-147.
Caputi, A. A. and Budelli, R. (2006). Peripheral electrosensory imaging by weakly electric fish. *J. Comp. Physiol. A* **192**, 587-600.
Caputi A. A., Macadar, O. and Trujillo-Cenóz, O. (1989). Waveform generation of the electric organ discharge in *Gymnotus carapo*. III: The electrogenic organ as an electric source. *J. Comp. Physiol. A.* **165**, 361-368.
Caputi, A. A., Budelli, R., Grant, K. and Bell, C. C. (1998). The electric image in weakly electric fish: physical images of resistive objects in *Gnathonemus petersii*. *J. Exp. Biol.* **201**, 2115-2128.
Caputi, A. A., Castelló, M. E., Aguilera, P. and Trujillo-Cenóz, O. (2002). Electrolocation and electrocommunication in pulse gymnotids: signal carriers, pre-receptor mechanisms and the electrosensory mosaic. *J. Physiol. Paris* **96**, 493-505.
Caputi, A. A., Aguilera, P. A. and Castelló, M. E. (2003). Probability and amplitude of novelty responses as a function of the change in contrast of the reafferent image in *G. carapo*. *J. Exp. Biol.* **206**, 999-1010.
Caputi, A. A., Carlson, B. A. and Macadar, O. (2005). The electric organs and their control. In *Electroreception* (ed. T. H. Bullock, C. D. Hopkins, A. N. Popper and R. R. Fay), pp. 410-452. New York, NY: Springer.
Caputi, A. A., Castelló, M. E., Aguilera, P. A., Pereira, C., Nogueira, J., Rodríguez-Cattaneo, A. and Lezcano, C. (2008). Active electroreception in *Gymnotus omari*: imaging, object discrimination, and early processing of actively generated signals. *J. Physiol. Paris* **102**, 256-271.
Caputi, A. A., Aguilera, P. A. and Pereira, A. C. (2011). Active electric imaging: body-object interplay and object's 'electric texture'. *PLoS ONE* **6**, e22793.
Castelló, M. E., Aguilera, P. A., Trujillo-Cenóz, O. and Caputi, A. A. (2000). Electroreception in *Gymnotus carapo*: pre-receptor processing and the distribution of electroreceptor types. *J. Exp. Biol.* **203**, 3279-3287.
Chen, L., House, J. L., Krahe, R. and Nelson, M. E. (2005). Modeling signal and background components of electrosensory scenes. *J. Comp. Physiol. A* **191**, 331-345.
Cilleruelo, E. R. and Caputi, A. A. (2012). Encoding electric signals by *Gymnotus omarorum*: heuristic modeling of tuberous electroreceptor organs. *Brain Res.* **1434**, 102-114.
Davis, E. A. and Hopkins, C. D. (1988). Behavioural analysis of electric signal localization in the electric fish, *Gymnotus carapo*, Gymnotiformes. *Anim. Behav.* **36**, 1658-1671.
de Perera, T. B. (2004). Fish can encode order in their spatial map. *Proc. Biol. Sci.* **271**, 2131-2134.
Gómez, L., Budelli, R., Grant, K. and Caputi, A. A. (2004). Pre-receptor profile of sensory images and primary afferent neuronal representation in the mormyrid electrosensory system. *J. Exp. Biol.* **207**, 2443-2453.
Green, D. M. and Swets, J. A. (1966). *Signal Detection Theory and Psychophysics*. New York: Wiley.
Heiligenberg, W. (1975). Electrolocation and jamming avoidance in the electric fish *Gymnarchus niloticus*. *J. Comp. Physiol.* **103**, 55-67.
Heiligenberg, W. (1976). Electrolocation and jamming avoidance in the mormyrid fish *Brienomyrus*. *J. Comp. Physiol.* **109**, 357-372.
Kalmijn, J. (1974). The detection of electric fields from inanimate and animate sources other than electric organs. In *Handbook of Sensory Physiology*, Vol. III (ed. A. Fessard), pp. 13-58. Berlin, Germany: Springer-Verlag.
Knudsen, E. I. (1975). Spatial aspects of the electric fields generated by weakly electric fish. *J. Comp. Physiol.* **99**, 103-118.
Lissmann, H. W. and Machin, K. E. (1958). The mechanism of object location in *Gymnarchus niloticus* and similar fish. *J. Exp. Biol.* **35**, 451-486.
Macadar, O. (1993). Motor control of waveform generation in *Gymnotus carapo*. *J. Comp. Physiol. A* **173**, 728-729.
MacIver, M. A. (2001). The computational neuroethology of weakly electric fish: body modeling, motion analysis and sensory signal estimation. PhD thesis, University of Illinois at Urbana-Champaign.
MacIver, M. A., Sharabash, N. M. and Nelson, M. E. (2001). Prey-capture behavior in gymnotid electric fish: motion analysis and effects of water conductivity. *J. Exp. Biol.* **204**, 543-557.
MacIver, M. A., Fontaine, E. and Burdick, J. W. (2004). Designing future underwater vehicles: principles and mechanisms of the weakly electric fish. *J. Oceanic Engineering, IEEE* **29**, 651-659.
MacIver, M. A., Patankar, N. A. and Shirgaonkar, A. A. (2010). Energy-information trade-offs between movement and sensing. *PLoS Comput. Biol.* **6**, e1000769.
Migliaro, A., Caputi, A. A. and Budelli, R. (2005). Theoretical analysis of pre-receptor image conditioning in weakly electric fish. *PLoS Comput. Biol.* **1**, e16.
Nelson, M. E. and MacIver, M. A. (1999). Prey capture in the weakly electric fish *Apteronotus albifrons*: sensory acquisition strategies and electrosensory consequences. *J. Exp. Biol.* **202**, 1195-1203.
Nelson, M. E. and MacIver, M. A. (2006). Sensory acquisition in active sensing systems. *J. Comp. Physiol. A* **192**, 573-586.

Pereira, A. C. (2009). Alcance espacial y efectos de contexto en el sentido eléctrico activo de *Gymnotus omari*. MSc thesis, University de la República, Montevideo, Uruguay.
Pereira, A. C. and Caputi, A. A. (2010). Imaging in electrosensory systems. *Interdiscip Sci.* **2**, 291-307.
Pereira, A. C., Centurión, V. and Caputi, A. A. (2005). Contextual effects of small environments on the electric images of objects and their brain evoked responses in weakly electric fish. *J. Exp. Biol.* **208**, 961-972.
Push, S. and Moller, P. (1979). Spatial aspects of electrolocataion in the Mormyrid fish *Gnathonemus petersii*. *J. Physiol.* **75**, 355-357.
Rasnow, B. (1996). The effects of simple objects on the electric field of *Apteronotus*. *J. Comp. Physiol. A* **178**, 397-411.
Rasnow, B. and Bower, J. M. (1996). The electric organ discharges of the gymnotiform fishes. I. *Apteronotus leptorhynchus*. *J. Comp. Physiol. A* **178**, 383-396.
Richer-de-Forges, M. M., Crampton, W. G. R. and Albert, J. S. (2009). A new species of *Gymnotus* (Gymnotiformes, Gymnotidae) from Uruguay: description of a model species in neurophysiological research. *Copeia* **2009**, 538-544.
Rother, D., Migliaro, A., Canetti, R., Gómez, L., Caputi, A. A. and Budelli, R. (2003). Electric images of two low resistance objects in weakly electric fish. *Biosystems* **71**, 169-177.
Schluger, J. H. and Hopkins, C. D. (1987). Electric fish approach stationary signal sources by following electric current lines. *J. Exp. Biol.* **130**, 359-367.
Sears, F. W. and Zemanski, M. W. (1955). *University Physics*, 2nd edn, pp. 1031. Reading, MA: Addison-Wesley.
Sicardi, A., Caputi, A. A. and Budelli, R. (2000). Physical basis of distance discrimination in weakly electric fish. *Physica A* **283**, 86-93.
Snyder, J. B., Nelson, M. E., Burdick, J. W. and Maciver, M. A. (2007). Omnidirectional sensory and motor volumes in electric fish. *PLoS Biol.* **5**, e301.
Stoddard, P. K., Rasnow, B. and Assad, C. (1999). Electric organ discharge of the gymnotiform fishes. III. *Brachyhypopomus*. *J. Comp. Physiol. A* **184**, 609-630.
Swets, J. A., Dawes, R. M. and Monahan, J. (2000). Psychological science can improve diagnostic decisions. *Psychol. Sci. Public Interest* **1**, 1-26.
von der Emde, G. (1990). Discrimination of objects through electrolocation in the weakly electric fish, *Gnathonemus petersii*. *J. Comp. Physiol. A* **167**, 413-421.
von der Emde, G. (1999). Active electrolocation of objects in weakly electric fish. *J. Exp. Biol.* **202**, 1205-1215.
von der Emde, G. and Engelmann, J. (2011) Active electrolocation. In *Encyclopedia of Fish Physiology: From Genome to Environment*, Vol. 1 (ed. A. P. Farrell), pp. 375-386. San Diego, CA: Academic Press.
von der Emde, G., Schwarz, S., Gomez, L., Budelli, R. and Grant, K. (1998). Electric fish measure distance in the dark. *Nature* **395**, 890-894.